Effect of Fluorination of the Hydrophilic Heads on Morphology and Molecular Structure of Langmuir Monolayers of Long-Chain Ethers

Jordan G. Petrov,*,† Gerald Brezesinski, Tonya D. Andreeva, and Helmuth Möhwald

Max-Planck Institute of Colloids and Interfaces, D-14476 Golm/Potsdam, Germany

Received: May 18, 2004; In Final Form: July 30, 2004

Brewster angle microscopy (BAM) and grazing incidence X-ray diffraction (GIXD) were used to compare morphology and molecular structure of Langmuir monolayers of docosyl trifluoroethyl ether (DFEE) and docosyl ethyl ether (DEE) on water. When spread at a molecular area of 70 Å^2/molecule both substances form islands of condensed phase and suspension of small 2D microcrystals attaching at the borderlines under compression. The DEE islands and the DEE monolayer at low surface pressure exhibit strong in-plane optical anisotropy, while the DFEE islands and the compact DFEE film are isotropic. The anisotropy of the DEE monolayer disappears at 10 mN/m, and above this surface pressure the monolayers with fluorinated and nonfluorinated heads are visually the same. The GIXD analysis identifies a L2′ phase with NNN molecular tilt and NN lattice distortion in the DEE islands and DEE monolayer at low surface pressure. The maximum tilt angle at zero compression is 22.6°. The islands and the compact DFEE film consist of closely packed upright molecules forming an S phase. At high surface pressure both monolayers have the same upright molecular arrangement with centered rectangular lattice and practically the same unit cell parameters and lattice distortion. Under such conditions the DFEE and DEE molecules occupy the same area of the water surface $A_{xy} = A_0 = 19.1$ Å^2. Since the van der Waals radius of the CF_3 group is by 16% larger as compared to that of the CH_3 group, the same A_0 value of the two films means a significantly thinner hydration shell of the fluorinated head. Substitution of the terminal CH_3 group in the DEE head by the CF_3 group in the DFEE head removes the low-pressure tilted phase and causes formation of the condensed phase of upright fluorinated molecules even at no compression. The decreased headgroup hydration of DFEE could be responsible for the upright versus tilted orientation of the DFEE and DEE molecules at low surface pressure. We suppose that the mechanism of the continuous tilting transition causing erection of the DEE chains is related to an increasing dehydration of the headgroups under compression.

Introduction

Fluorinated amphiphilic substances have become increasingly popular. They are used as strong surfactants in aqueous and nonpolar media, antifogging and antistatic films on glass, metal, and plastic surfaces, effective lubricants, and fire extinguishing agents.[1] Their biorelevant application spans between oil and fat repellents in cosmetics and oxygen carriers in artificial blood.[2] Mixed micelles, liposomes, Langmuir monolayers, and Langmuir−Blodgett multilayers of fluorinated and nonfluorinated surfactants show phase separation.[3] This behavior motivates their consideration as simple multicompartment multifunctional molecular aggregates modeling particular functions of living cells.[4]

The specific properties of fluorinated amphiphiles result from complete or partial *fluorination of their hydrocarbon chains*.[2−5] When the chains are long enough, the fluorinated amphiphiles form insoluble Langmuir monolayers at the air−water interface exhibiting unusual electrostatic and structural properties.[5,6] They display negative surface potential, in contrast to the positive ΔV values found for amphiphiles with nonfluorinated hydrophobic moiety.[5] This difference is due to the oppositely oriented C−F and C−H dipoles at the monolayer−air boundary. Monolayers with perfluorinated chains undergo only first-order phase transition between a dilute disordered phase and a condensed ordered phase,[6] while their analogues having hydrocarbon chains exhibit considerable polymorphism and a variety of first and second order phase transitions. Because of their strong hydrophobicity and stiffness the perfluorinated chains orient almost perpendicular to the water surface even at low surface pressures. Under the same conditions amphiphiles with hydrocarbon or partially fluorinated chains form tilted monolayer phases.[7]

In several studies[8] we began investigating a new family of amphiphiles with *fluorinated hydrophilic heads*. Since the monolayer−water boundary simulates the interface between a biomembrane and its environment, this location enables us to model the effect of fluorinated polar groups on membrane properties and functions. The dipole potential at this boundary regulates the transmembrane transport and binding of hydrophobic ions and the main goal of our investigations is to see how C−F dipoles in the headgroup affect these and other biorelevant processes. To better understand the effect of fluorination we compare two amphiphiles with the same hydrocarbon chains and the same hydrophilic head in which H-atoms were substituted by F-atoms. The first examined pair was trifluoroethyl behenate (TFEB) and ethyl behenate (EB). Negative dipole potential was found for monolayers of TFEB, while EB films showed the usual positive ΔV value.[8a] Parallel investigation of the mechanical properties, stability, morphology, and molecular structure of TFEB and EB monolayers were

* Address correspondence to this author, E-mail: jordan_g_petrov@yahoo.com.

† Permanent address: Institute of biophysics, Bulgarian Academy of Sciences, 1 Acad. G. Bonchev Str., 1113 Sofia, Bulgaria.

10.1021/jp047869e CCC: $27.50
Published on Web 09/22/2004

aimed at elaborating the mechanism of the sign reversal of the dipole potential due to fluorination of the hydrophilic heads, but the results obtained were insufficient.

In the present paper we compare monolayer morphology and molecular structure of an amphiphile with probably the simplest fluorinated head, the docosyl trifluoroethyl ether (DFEE), with those of its nonfluorinated analogue docosyl ethyl ether (DEE). Delineating the similarities and differences from the TFEB and EB films, having additional headgroup carbonyl dipoles, should help in understanding the structural origin of the dipole potential. Previous studies of phospholipid monolayers[9] via X-ray diffraction at grazing incidence (GIXD) have shown that replacement of the ester with ether chain linkages reduces the tilt angle in phosphatidylcholine films. On the other hand, the $C^{\delta+}{=}O^{\delta-}$ dipole yields a significant positive contribution to the dipole potential of Langmuir films of phospholipids, fatty acids, their esters with *n*-alcohols and glycerol, etc.,[10] so that one could expect that its removal would decrease the positive ΔV value of DEE and increase the negative ΔV value of DFEE as compared respectively to EB and TFEB films. In contrast to this expectation, we found a less negative dipole potential for DFEE versus TFEB monolayers and a more positive ΔV value for DEE versus EB films, which implies negative orientation of the carbonyl bond in the ethyl ester heads.[11]

Materials and Experimental Methods

Docosyl trifluoroethyl ether with MW 408.63 and docosyl ethyl ether with MW 436.35 were synthesized by Dr. D. Kurth and Mrs. C. Stolle at the Max-Planck Institute of Colloids and Interfaces, Golm/Potsdam, Germany. Details of the synthesis, purification, and characterization will be published elsewhere.[11] Elemental analysis for DFEE: C 70.59%, H 11.49%, F 13.91%. Calculated: C 70.54%, H 11.59%, F 13.95%. Elemental analysis for DEE: C 81.44%, H 14.63%. Calculated: C 81.28%, H 14.21%. DEE forms white crystals with a melting point of 45°C, while DFEE is a white wax.

Both substances were dissolved in J. T. Baker chloroform to a concentration of 1 mM and aliquots of these solutions were spread on the water surface. Milli-Q-Millipore water was used as liquid substrate. After 5 min, for evaporation of the solvent, the monolayers were compressed at 2.2 Å^2/(molecule·min). During the measurements the aqueous substrate was kept at 20 ± 0.1 °C via a temperature-control system.

The surface pressure−molecular area isotherms π/A were recorded on a Langmuir film balance with a Teflon trough and Wilhelmy dynamometric system. The morphology of the DFEE and DEE films was studied with a Brewster angle microscope BAM-2 (NFT, Göttingen, Germany). *p*-polarized green light from a 135-mW semiconductor laser was directed at the Brewster angle to the pure water surface giving zero reflectivity. Spreading of the monolayer or varying its density gives rise to reflected light registered by a CCD camera and visualized by a monitor. Since only the middle part of the optical field is well focused an adjustable objective and special software are used to equalize the focus of scanned stationary images.

An optical anisotropy of the monolayer, due to specific molecular structure or collective molecular tilt, can be detected via an analyzer in the pathway of the reflected beam. Parallel analyzer and polarizer yield maximum intensity, while crossed position enables best optical contrast. Thus, a pure water surface or a homogeneous film appears bright with a parallel analyzer, while a crossed analyzer gives a dark optical field.

Compression of the monolayer was recorded on a videotape, and the images were digitized and transformed to frames 630 × 472 μm by a frame grabber and a computer. Simultaneously recorded π/t and A/t dependencies were used to ascribe each image to the corresponding surface pressure and molecular area.

The molecular structure of the monolayers was studied by means of a liquid surface diffractometer at the undulator beam line BW1, HASYLAB, DESY, Hamburg, Germany. A monochromatic X-ray beam strikes the water surface at a grazing incidence of $0.85\alpha_c$, where $\alpha_c = 0.13°$ is the angle of total external reflection. The scattered radiation is detected via a linear position-sensitive detector as a function of the vertical scattering angle. The accumulated position-resolved counts are corrected for polarization, effective area, and powder averaging (Lorenz factor). The Yoneda−Vineyard peak is used to determine the detector position.

The horizontal component Q_{xy} of the scattering vector (Bragg peaks) accounts for the periodicity in the monolayer plane. From the positions of the Q_{xy} maxima one calculates the repeat distances d_{hk} of the film lattice for each couple of Miller indices (h,k):

$$d_{hk} = \frac{2\pi}{Q_{xy}^{hk}} \tag{1}$$

The values of d_{hk} yield the parameters of the primitive unit cell in the water surface $a, b, c, \alpha, \beta, \gamma$. This lattice is determined by the collective tilt of the hydrocarbon chains or the conformation of the hydrophilic heads if their cross-section exceeds that of the chains. The lattice in the plane normal to the chains eliminates the effect of the tilt.

The out-of-plane component Q_z of the scattering vector (Bragg rods) yields the orientation of the monolayer molecules. The tilt angle θ and the tilt azimuth ψ can be determined from the two peaks of the centered rectangular cell:

$$Q_z^{hk} = Q_{xy}^{hk} \cos \psi_{hk} \tan \theta \tag{2}$$

When the maximum scattering intensity is located at $Q_z = 0$ the monolayer molecules are upright. If they are tilted, the Bragg rod maxima appear at the nonzero Q_z-position, which depends on direction and magnitude of the tilt. A centered rectangular unit cell with NN tilt (to next neighbors), shows one nondegenerate in-plane peak Q_{xy}^{n} at $Q_z = 0$ and one 2-fold degenerate peak Q_{xy}^{d} at $Q_z > 0$. For NNN tilt (to next-nearest neighbors), the degenerate and nondegenerate in-plane peaks have nonzero Q_z values in a ratio 2:1.

A rectangular lattice is better characterized by the rectangular parameters $a_r = a$, $b_r = 2b \cos(\gamma - 90°)$, and the area per molecule in the water surface $A_{xy} = a_r b_r/2$. The area per molecule in the plane normal to the chains A_0 is related to A_{xy} by the relationship:

$$A_0 = A_{xy} \cos \theta \tag{3}$$

The full width of the in-plane peak at half-maximum ΔQ_{xy} gives the position correlation length ζ in the XY plane. For a polycrystalline monolayer treated as 2D-powder ζ reads:

$$\zeta = \frac{1.8\pi}{\Delta Q_{xy}^{hk}} \tag{4}$$

The intrinsic peak width ΔQ_{xy} that should be substituted in eq 4 can be obtained by correcting the measured width by the instrumental resolution, $(\Delta Q_{xy})^2 = (\Delta Q_{xy,\mathrm{msd}})^2 - (\Delta Q_{xy,\mathrm{ins}})^2$.

Amphiphilic molecules with small hydrophilic heads pack in a hexagonal phase with upright orientation of the chains at

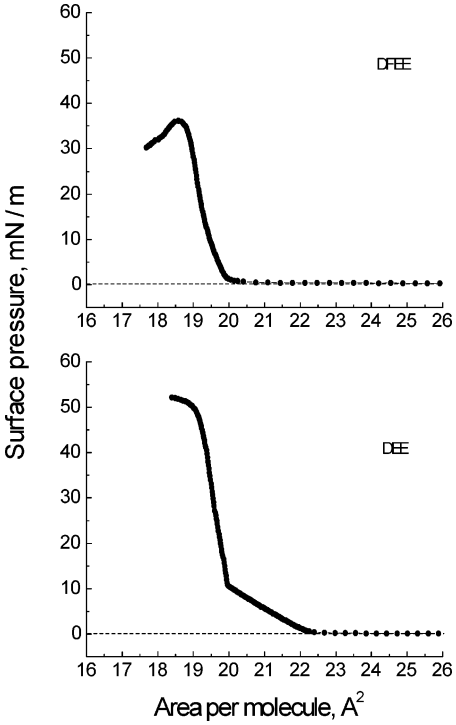

Figure 1. Surface pressure−molecular area isotherms of DFEE and DEE.

intermediate surface pressure and temperature. At lower pressure and higher temperature they may tilt and the hexagonal lattice may transform to a centered orthorhombic (rectangular) lattice. The magnitude ξ of the lattice distortion is given by

$$\xi = \frac{l_l^2 - l_s^2}{l_l^2 + l_s^2} \tag{5}$$

where l_l and l_s are the long and the short axes, respectively, of the ellipse passing through the six nearest neighbors of a given molecule; they can be calculated from the values of d_{hk}. If the molecular rotation is hindered by lower temperature, higher surface pressure, or stronger attraction between chains, the C−C bonds of adjacent molecules form a "herringbone" arrangement that also causes a lattice distortion.

Results

Surface Pressure−Area Isotherms. π/A isotherms of DFEE and DEE monolayers are shown in Figure 1. The collapse surface pressure of the DFEE monolayer is significantly lower than that for the DEE film, while the molecular areas at collapse are close to each other. (In this case π_{col} and A_{col} were determined via linear extrapolation of the adjacent parts of the isotherm.) At the compression velocity used the mean values averaged from five isotherms are 40.0 ± 2.1 mN/m and 18.5 ± 0.1 Å^2 for DFEE, and respectively 52.3 ± 2.4 mN/m and 18.9 ± 0.2 Å^2 for DEE. The coordinates of the inflection points of the isotherms, π_{inf} and A_{inf}, where $d^2\pi/dA^2$ reverses sign and the monolayers lose stability, show the same relationship: π_{inf} = 24.2 ± 2.0 mN/m (DFEE) vs 41.3 ± 1.9 mN/m (DEE) and A_{inf} = 19.1 ± 1.0 Å^2 (DFEE) vs 19.5 ± 0.2 Å^2 (DEE). Since both amphiphiles have the same hydrocarbon chains the decrease of π_{col} and π_{inf} results from fluorination of the heads. The larger values of A_{col} and A_{inf} for DEE mean more or larger voids because the CF_3 terminals of the fluorinated heads are larger than the CH_3 terminals of the nonfluorinated ones (see the BAM and GIXD data in the next sections).

The isotherm of DFEE has no plateaus or clearly expressed kinks that would indicate first or second order phase transitions. Instead of that it shows a gradual transition from a more shallow low-pressure section to a steeper high-pressure part. In contrast, the isotherm of DEE in Figure 1 has a sharp kink at 10.6 mN/m and 20.0 Å^2. Extrapolation of the high- and low-pressure parts toward the abscissa gives the molecular areas at zero compression of the upright phase, $A_{ext,\perp}$, and the tilted phase, $A_{ext,tilt}$. Their ratio yields the maximum tilt angle at zero compression θ_{max}:

$$\cos\theta_{max} = \frac{A_{ext,\perp}}{A_{ext,tilt}} \tag{6}$$

Substituting the values of $A_{ext,\perp}$ = 20.2 Å^2 and $A_{ext,tilt}$ = 22.3 Å^2 for DEE gives θ_{max} = 25.1°.

Morphology of DFEE and DEE Monolayers. Scanned images of DFEE and DEE films at different degrees of compression are shown in Figure 2. The left-hand side corresponds to a DFEE monolayer and the right-hand side refers to the DEE film. When spread at an initial molecular area of 70 Å^2 both substances form islands of 2D condensed phase, including dark areas with a nonreflecting gaseous phase. The DFEE islands contain more voids than the DEE ones. When the film area is diminished, the islands organize in "archipelagos" with sharp "coast lines" for the DFEE film, and smoother ones for the DEE monolayer (cf. Figure 2, parts a and a′). Further compression decreases the partial area of the voids and makes the monolayers denser. At this stage one observes a 2D suspension of microcrystals, which attach to the "coast lines". At high surface pressure a homogenization of the monolayers occurs and both films appear compact (Figure 2b,b′). Occasionally, intermediate states, "lakes" almost covered by 2D suspension, can be seen in both films at nonzero surface pressures (Figure 2b). The growth of the compact parts of the films via attachment of microcrystals at the "coast lines" and the progressive closing of the "lakes" under compression imply polycrystallinity of both monolayers.

When visually following the monolayer compression on the BAM monitor one finds that the movement of the islands sharply slows down practically together with the initial surface pressure increase in the π/A isotherms. Such coincidence suggests that π rises when the compact domains are brought together. Further compression homogenizes the DFEE and DEE films via 2D sintering.

The compact parts of the heterogeneous DFEE monolayer (Figure 2a), as well as the homogeneous DFEE film (Figure 2b), are optically isotropic. This conclusion was checked via rotation of the analyzer at 0.2, 6.0, and 20 mN/m, which did not show the characteristic changes of reflected light. The DEE monolayer exhibits an optical anisotropy at low surface pressure, confirmed via rotation of the analyzer at different degrees of compression (Figure 3). The first column shows BAM images obtained with parallel polarizer and analyzer; crossed polarizer and analyzer give the images in the second column. At molecular areas of 40−50 Å^2 one finds the characteristic dark-bright changes of the monolayer domains (Figure 3a,a′). After the initial increase of the surface pressure the irregular domains (Figure 3a,a′) transform to parallel strips (Figure 3b,b′) and the anisotropy of this texture weakens with increasing surface pressure and disappears at 10−11 mN/m. McConnell[12] related such texture transformations of solid domains to a limited

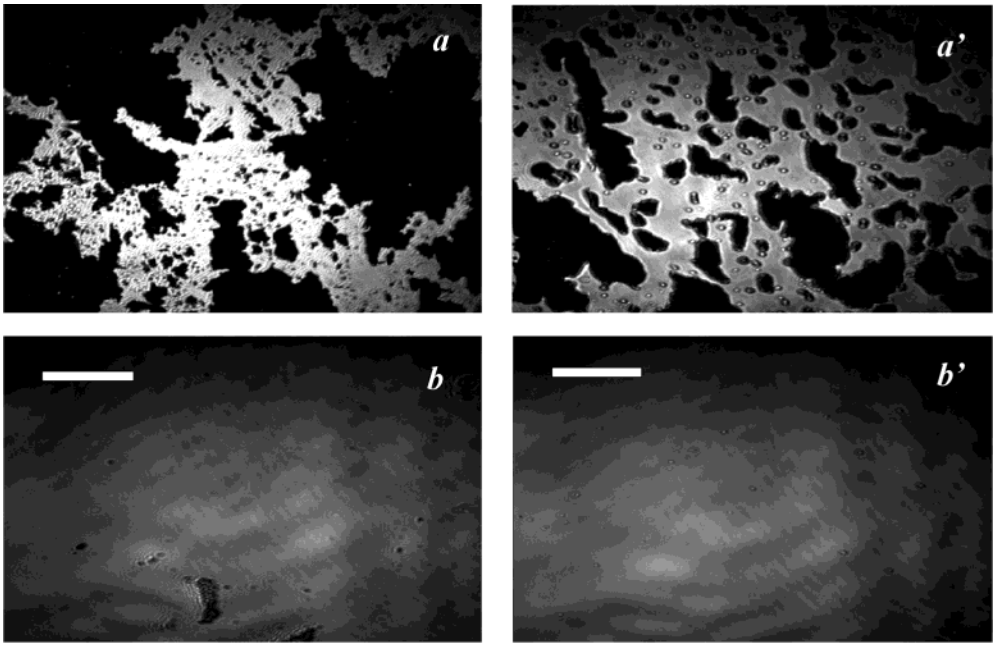

Figure 2. Comparison of the morphology of DFEE (left) and DEE (right) monolayers at different degrees of compression: DFEE (a) 0.2 mN/m and 33 Å^2 and (b) 6.0 mN/m; DEE, (a′) 0.3 mN/m and 32 Å^2 and (b′) 6.0 mN/m. The white bars correspond to 100 μm.

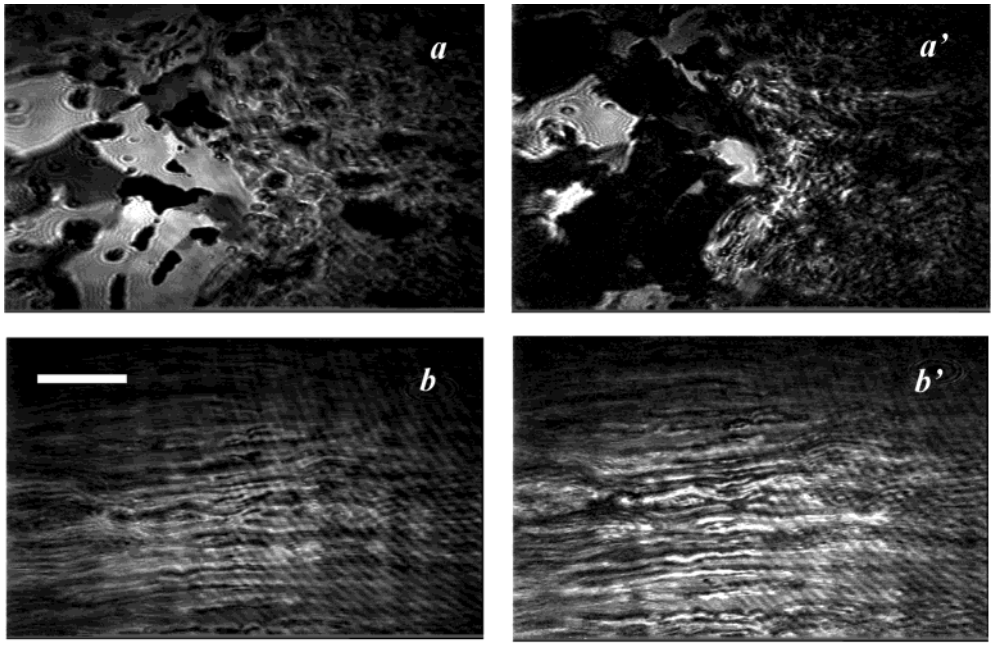

Figure 3. Optical anisotropy of the DEE monolayer at low surface pressure. The left side images correspond to crossed polarizer and analyzer, the right ones to parallel polarizer and analyzer. Images a and a′: 0.2 mN/m and 26 Å^2. Images b and b′: 6.0 mN/m. The white bar corresponds to 100 μm.

nucleation rate and electrostatic instability resulting from competition of line tension and dipole−dipole repulsion.

Molecular Structure of DFEE and DEE Monolayers. Contour plots of the diffraction peaks of DFEE and DEE monolayers are shown in Figure 4. They present the scattered intensity versus the in-plane Q_{xy} and out-of-plane Q_z components of the scattering vector. The left-hand plot corresponds to a DFEE film at 7.0 mN/m, and the right-hand plots show the DEE film at 7.0 mN/m (bottom) and 13.8 mN/m (top). The two peaks on each plot imply centered rectangular lattices. For the DFEE monolayer both reflections are located at $Q_z = 0$ Å^{-1}, which means that at 7.0 mN/m the molecules of DFEE are upright. At the same surface pressure, the DEE film gives two Bragg peaks located at $Q_z > 0$. Such location indicates a tilt to the next-nearest neighbors. At $\pi = 13.8$ mN/m both in-plane reflexes of DEE are shifted to zero Q_z. This shift indicates a transition from a NNN tilted phase to an upright phase occurring between 7.0 and 13.8 mN/m.

To more precisely locate the phase transition in the DEE film, and to check if similar transitions occur in the DFEE monolayer below 7.0 mN/m we have recorded the diffraction peaks for both systems at different π-values (Tables 1S−3S, see the Supporting Information). The positions of the obtained low-order maxima for DFEE monolayer show that even at 0.2 mN/m $Q_z\{11\} = Q_z\{02\} = 0$. Therefore, the DFEE monolayer forms an untitled phase even before the initial increase of surface pressure and this molecular orientation is retained at 7.0 and 20 mN/m. The calculated and experimental maxima of the three

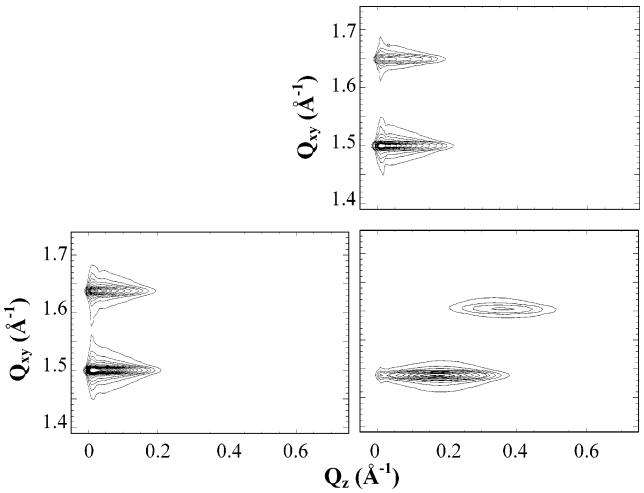

Figure 4. Contour plots of the scattered X-ray intensities as function of the in-plane Q_{xy} and out-of-plane Q_z scattering vectors. Left: DFEE monolayer at 7.0 mN/m. Right bottom: DEE monolayer at 7.0 mN/m. Right top: DEE monolayer at 13.8 mN/m.

higher order peaks have even sums of the *h*,*k*-indices (Table 2S).

For DEE monolayers one finds nonzero $Q_z\{11\}$and $Q_z\{02\}$ indicating a NNN tilted phase between 0.3 and 9.0 mN/m (Table 3S). Larger Q_z^{hk} correspond to larger Q_{xy}^{hk} values, and the ratio $Q_z\{02\}$:$Q_z\{11\}$ remains always 2:1. This implies NN distortion of the monolayer lattice, which, together with the NNN tilt azimuth, characterizes the L2′ phase. Both $Q_z\{11\}$ and $Q_z\{02\}$ decrease with increasing π, because of the decreasing of tilt angle. At high surface pressure $Q_z\{11\}= Q_z\{02\}= 0$, indicating formation of an upright, most probably S phase. Their values are almost constant and very close to those for the DFEE monolayer.

The variation of the in-plane lattice parameters a_r and b_r with surface pressure is shown in Figure 5. The increase of a_r and respective decrease of b_r for the upright phase of the DFEE monolayer (see the squares) could result from rotation of the chains to achieve a herringbone arrangement or from conformational changes or denser packing of the fluorinated heads. For the DEE monolayer (the circles) b_r strongly decreases below 9.9 mN/m due to uprighting of the chains and remains almost constant above this value. At 20 mN/m one finds $a_r = 5.01$ Å for both films, and $b_r = 7.63$ Å for DFEE, respectively 7.62 Å for DEE. Therefore, at high surface pressure the monolayers of the fluorinated and nonfluorinated ethyl ether have practically the same molecular structure.

Extrapolation of the high-pressure parts of the a_r/π and b_r/π dependences of the ethyl ether monolayers to $\pi = 0$ (see the dotted lines) would give the unit cell parameters of an imaginary phase of upright DEE molecules at zero surface pressure. The values thus obtained, $a_r(0) = 5.017$ Å (DEE) and $b_r(0) = 7.654$ Å (DEE), differ from $a_r(0) = 4.995$ Å (DFEE) and $b_r(0) = 7.696$ Å (DFEE) of the upright phase of the fluorinated ether, but their product gives the same molecular area at no compression, $A_{xy}(0) = 19.20$ Å^2.

The 1/cos θ vs π data in Figure 6 show that the vertical molecular orientation in the DFEE film does not depend on surface pressure. The same plot for the DEE monolayer consists of a linear decrease and a plateau intersecting at 9.9 mN/m. The two branches correspond to decreasing and zero-tilt angles, respectively. Extrapolation of the low-pressure section to $\pi = 0$ gives $\theta_{max} = 22.6°$ that significantly differs from $\theta_{max} = 25.1°$

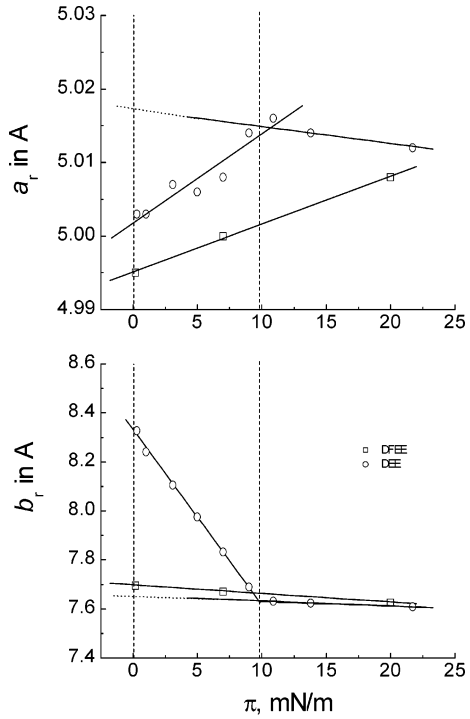

Figure 5. Variation of the parameters of the rectangular lattices of DFEE and DEE films with increasing surface pressure. Squares represent DFEE data and circles DEE data. The dashed line at 9.9 mN/m indicates the end of the L2′-S phase transition in the DEE monolayers.

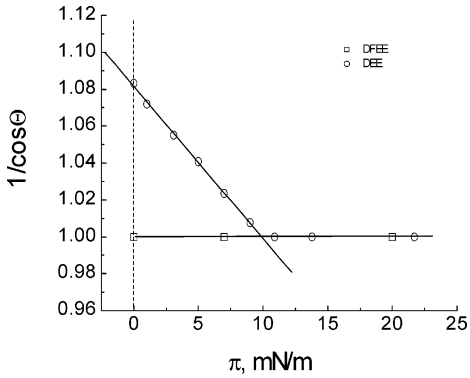

Figure 6. Dependence of the tilt angle θ on surface pressure presented in $(\cos \theta)^{-1}/\pi$ scale. The squares (DFEE) show no tilt between 0 and 20 mN/m, and the circles (DEE) illustrate decreasing tilt angle and upright orientation above 9.9 mN/m.

obtained from the π/A isotherm in Figure 1. The reason for this is the incomplete homogenization of the DEE monolayer.

The A_{xy}/π dependencies for DFEE and DEE films are presented in Figure 7 (top). For DFEE there is no sharp change of A_{xy} showing tilting transition. The different slopes of the low- and high-pressure sections of the DEE data indicate the L2′-S tilting transition completed at 9.8 mN/m. The coincidence of the high-pressure A_{xy} values of both monolayers confirms the same molecular packing under such conditions. Moreover, the low-pressure values for DFEE fall on the extrapolation of the straight line drawn through the high-pressure A_{xy} values of DEE, confirming the above conclusion that upright DFEE and DEE molecules would occupy the same area $A_{xy}(0)$ at zero compression.

The area per molecule in the plane perpendicular to the chains excludes the effect of the molecular tilt. Figure 7 (bottom) shows the dependence of A_0 on surface pressure for DFEE (squares) and DEE (circles). It can be seen that above 5.0 mN/m the value

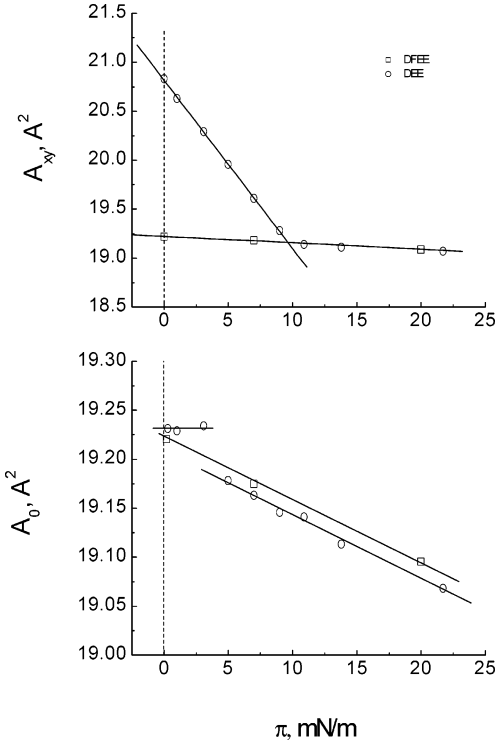

Figure 7. Surface pressure dependencies of the area per molecule on the water surface A_{xy} (top) and in the plane perpendicular to the chains A_0 (bottom).

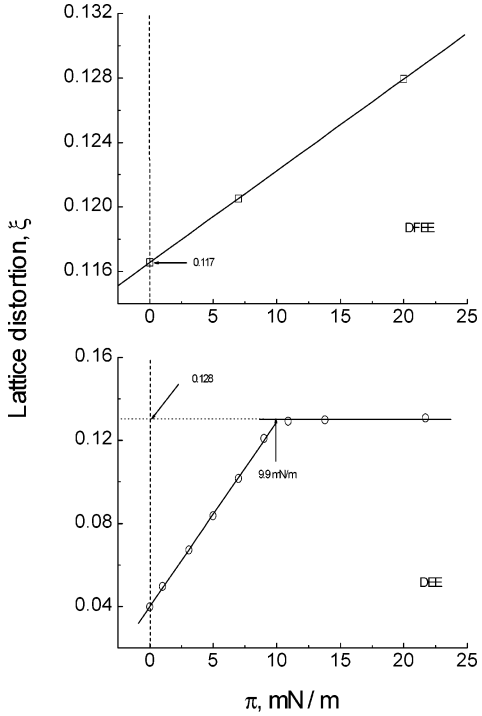

Figure 8. Distortion ξ of the in-plane lattice of DFEE (top) and DEE (bottom) monolayers as a function of surface pressure. The low- and high-pressure sections of the DEE dependence correspond to the tilted and the upright phase. Extrapolation of the high-pressure section to $\pi = 0$ gives a larger distortion at no compression for DEE, $\xi_0 = 0.128$, as compared to $\xi_0 = 0.117$ for DFEE.

of A_0 per DFEE chain is larger than A_0 per DEE chain, but this relation reverses between 5.0 and 3.1 mN/m. It is curious that the above singularity occurs in the surface pressure interval where transformation from irregular domains to stripe-like texture is observed (Figure 3).

Figure 8 shows the variation of the in-plane lattice distortion ξ of DFEE (top) and DEE (bottom) monolayers with surface pressure. The distortion of the DFEE monolayer lattice increases with increasing π. Since the fluorinated molecules stay upright already at 0.2 mN/m (Figure 6) this increase should originate either from a "herringbone" arrangement of the chains or from conformational change or optimal packing of the headgroups. The strong initial increase of the distortion of the DEE lattice (note the scale difference) accompanies the decrease of molecular tilt. Above 9.9 mN/m ξ of this lattice changes just slightly, again indicating a variation of the lattice distortion of the untilted phase with surface pressure. At high surface pressure the same upright chains of DFEE and DEE pack in practically the same distorted lattice; at 20 mN/m $\xi = 0.128$ for DFEE vs 0.130 for DEE. However, the lattice distortion, which the upright phase of DEE would have at no compression (obtained via extrapolation of the high-pressure ξ/π dependence to $\pi = 0$), is significantly larger than the zero-pressure distortion of the DFEE upright lattice, ξ_0(DEE) = 0.128 versus ξ_0(DFEE) = 0.117. Therefore, despite the same hydrocarbon chains, uncompressed upright DEE molecules would cause stronger deviation from the hexagonal symmetry as the upright DFEE molecules. If one assumes that the slope $d\xi/d\pi$ characterizes the deformability of the lattice of the upright phases, the values of $(5.69 \pm 0.03) \times 10^{-4}$ for DFEE versus $(1.73 \pm 0.33) \times 10^{-4}$ for the DEE high-pressure part show that the same external force causes larger lattice distortion of the fluorinated monolayer.

It is known[7] that in the tilted L2′ phase the degenerated peak is narrower than the nondegenerated peak, and that both fwhm decrease with increasing surface pressure. This tendency remains in the upright S-phase, because of the continuous character of the L2′-S transition.[7] We also found anisotropy of the position correlation length of the L2′-phase of the DEE monolayer; the values of $\zeta\{11\}$ in the NN direction are larger as compared with the correlation length $\zeta\{02\}$ in the NNN direction (Table 1). The ζ values of the upright DFEE and DEE phases are shown in Table 2. They suggest crystalline order increasing under compression and anisotropy of the lattice distortion in both cases.

TABLE 1: Positional Order of the Tilted L2′ Phase of the DEE Monolayer at Different Surface Pressures

π [mN/m]	$\zeta\{11\}$ [Å]	$\zeta\{02\}$ [Å]
0.3	445	165
1.0	445	165
3.1	490	175
5.0	490	220
7.0	630	275
9.0	750	350

TABLE 2: Positional Order of the Upright Phases of DFEE and DEE Monolayers at Different Surface Pressures

monolayer	π [mN/m]	$\zeta\{11\}$ [Å]	$\zeta\{02\}$ [Å]
DFEE	0.2	750	375
DFEE	7.0	750	550
DFEE	20.0	1370	750
DEE	10.9	1370	550
DEE	13.8	1370	750
DEE	21.7	1370	1370

Heterogeneity of DFEE and DEE Monolayers. Comparison of the π/A isotherms determined via Langmuir balance with the π/A_{xy} isotherms resulting from the GIXD measurements shows that the π/A curves are shifted to larger areas. It is interesting that the π/A and π/A_{xy} isotherms of the DFEE monolayer merge at the inflection point, where monolayer loses stability. This coincidence explains why the collapse molecular area $A_{col} = 18.5$ Å^2 is below the area of the closely packed

TABLE 3: Area Fraction of the Voids in DFEE and DEE Monolayers at Different Surface Pressures

monolayer	π [mN/m]	A [Å^2]	A_{xy} [Å^2]	$(A - A_{xy})/A$ [%]
DFEE	0.2	23.0	19.2	16.5
DFEE	7.0	19.6	19.2	2.0
DFEE	20.0	19.2	19.1	0.5
DEE	0.3	23.0	20.8	9.6
DEE	7.0	20.7	19.6	5.3
DEE	19.5	19.8	19.1	3.6

upright molecules determined via GIXD, $A_{GIXD} = 19.1$ Å^2. In the case of the DEE monolayer $A_{GIXD} = 19.1$ Å^2 coincides with the average molecular area 18.9 ± 0.2 Å^2 obtained via linear extrapolation of the high-pressure part of the isotherm and the section where the collapse is significant.

Table 3 compares the area fraction $(A - A_{xy})/A$ of the voids in the DFEE and DEE monolayers. At 0.2−0.3 mN/m and average area $A = 23$ Å^2 the DFEE film contains more voids than the DEE monolayer, but homogenizes more easily; at ∼20 mN/m $(A - A_{xy})/A = 0.5\%$ for DFEE and 3.6% for DEE.

Discussion

Comparison of Morphology and Molecular Structure of DFEE and DEE Monolayers. Both DFEE and DEE form large incompact islands of condensed phase and suspensions of small 2D microcrystals attaching at the coastlines under compression. At a low degree of compression black areas ("lakes") can be seen in both monolayers; they become gray and disappear at high surface pressure. The disappearance of the "lakes" implies mobility of the monolayer subunits (2D microcrystals), which seem to retain their autonomy even in visually homogeneous films.

The DFEE islands and the compact DFEE film are isotropic, while the DEE islands and the DEE monolayer at low surface pressure exhibit strong in-plane optical anisotropy. The GIXD analysis shows that both the islands and the compact DFEE consist of closely packed upright molecules. The DEE monolayers form a L2′ phase at low surface pressure with NNN tilt and maximum tilt angle of 22.6° at zero compression. The tilting L2′-S or L2′-CS transition is completed at 10 mN/m. In the high-pressure phase the DFEE and DEE molecules occupy the same area $A_{xy} = A_0 = 19.1$ Å^2. Because of the larger van der Waals volume of 35.4 Å^3 of the CF_3 group as compared to the van der Waals volume 22.7 Å^3 of the CH_3 group[13] the same molecular area of the upright DFEE and DEE molecules means a significantly thinner hydration shell of the fluorinated head. This conclusion is supported by the lower collapse pressure of the DFEE films.

Comparison of the Effect of Headgroup Fluorination on Morphology and Molecular Structure of Ethyl Ester and Ethyl Ether Monolayers. There is no qualitative difference in morphology of DFEE versus TFEB and DEE versus EB monolayers. Both ester and ether films behave as described in the previous section of the discussion. The centered rectangular unit cell is the common symmetry of all four (fluorinated and nonfluorinated) monolayers, probably due to the same hydrocarbon chains of the amphiphiles. However, the islands and the compact DFEE and TFEB films consist of upright molecules, while DEE and EB monolayers form L2′ tilted phases at low surface pressure. The tilt angles at zero compression are different, 22.6° for DEE and 17.6° for EB, respectively. In the high-pressure S or CS phase the fluorinated and nonfluorinated amphiphiles of the given couple occupy the same area of the water surface despite the larger van der Waals volume of the CF_3 as compared to the CH_3 group.[13] Curiously, the simpler headgroup of the ethers yields larger molecular area $A_0 = 19.1$ Å^2 in upright orientation, as compared to $A_0 = 18.9$ Å^2 obtained for TFEB and EB monolayers at high surface pressure. On the other hand, both values exceed the cross-section $A_0 = 18.2$ Å^2 of an ethyl stearate molecule in nonhydrated 3D crystals.[14]

Substitution of the CH_3 by a CF_3 terminal of the heads removes the strong in-plane optical anisotropy observed at low surface pressures for both nonfluorinated DEE and EB monolayers. The anisotropy of the DEE film completely disappears after the L2′-S transition, while the EB monolayer remains weakly anisotropic in the upright phase. Seven high-order peaks obtained for TFEB versus three such peaks for DFEE imply better crystalline structure of the monolayer with trifluoroethyl ester heads. The in-plane peaks of both ester monolayers are resolution limited, i.e., their position correlation lengths exceed the highest value of 1370 Å found for $\zeta\{11\}$and $\zeta\{02\}$ of the fluorinated and nonfluorinated ethyl ether films.

The parameters of the upright phases are almost the same for monolayers of the same chemical type, i.e., the high surface pressure monolayer structure does not depend on fluorination of the heads. On the other side, the lattice parameters of the ester and ether couples significantly differ from each other, clearly demonstrating that different hydrophilic heads cause different packing of (almost) the same hydrocarbon chains.

Effect of the Size of the Hydrated Headgroup on the Tilt of the Hydrocarbon Chains. The semiempirical quantum-mechanical maps of molecular lipophilicity of trifluoroethyl behenate and ethyl behenate molecules in vacuo[8b] show that substitution of the $-CH_3$ group in the $-COOCH_2CH_3$ head by a $-CF_3$ group significantly decreases the hydrophilicity of the ester head. A similar effect should be expected for the DFEE and DEE couple, where fluorination substitutes the terminal $-CH_3$ group of the $-OCH_2CH_3$ head by a $-CF_3$ group. Such a difference in hydration of the fluorinated and nonfluorinated heads could be responsible for the low-pressure structural differences of the DFEE and TFEB versus DEE and EB monolayers, respectively.

McIntosh[15] explained the upright chains of DPPE and the tilted chains of DPPC in hydrated suspensions through different sizes of the hydrated phosphatidylcholine and ethanolamine heads. The DPPC chains are tilted at approximately 30° from the normal to the bilayer, while those of DPPE are almost perpendicular to it. The smaller hydrated heads of DPPE enable close approach of the vertical chains to a distance where the attraction between them equilibrates with the steric repulsion. For the larger hydrated heads of DPPC simultaneous close packing of the heads and upright chains is impossible; in this case the strong attraction between the chains causes their tilt to ensure enough room for the heads at the water surface. Beyond pure DPPC bilayers, McIntosh[15] studied mixtures of DPPC with tetradecane or DPPC with La^{3+} dissolved in the aqueous phase. No tilt was found with both additives. The loss of the tilt was related to penetration of tetradecane molecules between the DPPC chains and increase of their van der Waals attraction in the upright position. The effect of La^{3+} was explained via conformational changes of the DPPC head, reducing its cross-section.

This model explains many other structural data with lipid bilayers. Levine[16] found that the tilt angle in DPPC bilayers depends on humidity. At 2% water content, the hydrocarbon chains were vertically oriented, but at 20% water a limiting angle of 28° was found. Tardieu et al.[17] observed an increase of the tilt angle from 17° to 33° with increasing the molar fraction of water in the same system. Hui[18] obtained a tilt angle of 16° for

hydrated oriented PC multilayers, but no tilt in dehydrated single bilayers. Such an increase of the tilt angle with increase of the water content can be rationalized via increased hydration, respectively size of the hydrated PC headgroup. On the other hand vertical chains are typical for completely hydrated gel phases of ethanolamines.[15,19,20] Such orientation fits the above picture if one recalls the lower hydration number, respectively smaller size of the PE head as compared to the PC head.[21]

After development of the GIXD technique a similar effect of the size of the hydrated head on the tilt of the hydrocarbon chains was registered for Langmuir monolayers at the air−water and oil−water interface. Brezesinski et al.[22] investigated DPPC and DPPE films at both interfaces. Tilt angles of 28° and 24° were found for DPPC on water at 30 and 45 mN/m, respectively, but the tilt disappeared when dodecane or hexadecane were used as the outer phase (see Figure 7 of ref 22). The specific adsorption of phospholipase A_2 (PLA_2) at the headgroups of a monolayer of the D-enantiomer of DPPC, which is recognized but not cleaved by the enzyme, also causes erection of the DPPC chains.[23] Since specific adsorption of dissolved species at monolayers is usually accompanied by dehydration of the heads, the effect of PLA_2 fits the above scenario. Both results are in qualitative accordance with the McIntosh data[15] for the effect of alkanes and La^{3+} on the orientation of chains in DPPC bilayers, but this agreement should be considered with caution, because the presence of the second monolayer sometimes yields interdigitated phases.

Weidemann and Vollhardt[24] investigated monolayers of dipalmitoyl phospholipids with different numbers of $-CH_3$ groups in the head. They compared DPPC having $-N(CH_3)_3$ terminal, DPP(Me_2)E with $-NH(CH_3)_2$ terminal, DPP(Me)E with $-NH_2CH_3$ terminal, and DPPE with $-NH_3$ terminal. It was found that the monolayers of DPPC and DPP(Me_2)E have tilted chains even at high surface pressure. Complete erection of the chains was registered in DPP(Me)E monolayers, but it occurred at significantly higher surface pressure than for DPPE films. The authors[24] related the tilt of the hydrocarbon chains to the size of the hydrated headgroups, which decreases in the above sequence. Their paper shows also another interesting correlation: larger tilt corresponds to higher collapse pressure. DPPC films do not collapse up to 72 mN/m, while π_{col} of the other monolayers decreased in the following sequence: π_{col} of DPP(Me_2)E > π_{col} of DPP(Me)E > π_{col} of DPPE. This correlation points to a decreasing affinity of the heads toward water, respectively decreasing hydration in the heads in the direction from DPPC toward DPPE.

Comparison of the molecular structure of palmitic acid, methyl palmitate, and ethyl palmitate monolayers in the condensed state showed a systematic change with decreasing hydrophilicity of the headgroup at constant molecular area.[25] The maximum tilt angle at zero compression decreased from 33° for palmitic acid to 16° for ethyl palmitate. The size of the unhydrated head increases in this direction because of substitution of −OH in the −COOH group of the palmitic acid through $-OCH_3$ in methyl palmitate and $-OCH_2CH_3$ in ethyl palmitate. However, the hydrophilicity of the headgroups decreases in the same direction so that one could speculate that the observed decrease of the tilt angle correlates with the size of the hydrated heads.

The above analysis of bilayer and monolayer structure shows that hydration of the polar heads increases their size causing a tilt of the hydrocarbon chains, which energetically optimizes the structure. Weaker hydrated heads have smaller and less tilted or upright chains. Such monolayers are usually less stable and collapse at lower surface pressure. In this context the decreased hydrophilicity of the trifluoroethyl group might be the reason for the vertical orientation of the DFEE and TFEB chains even at zero surface pressure. Under the same conditions the DEE and EB molecules having more hydrophilic, respectively larger, heads are tilted toward next-nearest neighbors. In the vertical phase the DFEE and DEE molecules occupy the same area of 19.1 Å^2, which is close to A_0 = 18.9 Å^2 for the TFEB−EB couple. This value exceeds the cross-section area 18.2 Å^2 of a vertical chain in unhydrated EB crystals,[14] suggesting that hydration of the heads changes their conformation. The 16% larger van der Waals radius of the $-CF_3$ group, as compared to the $-CH_3$ group, and the same molecular area at high surface pressure imply thinner hydration shells of the $-COOCH_2CF_3$ versus $-COOCH_2CH_3$ and $-OCH_2CF_3$ versus $-OCH_2CH_3$ groups.

The Tilting Transition and Headgroup Dehydration Process. Our present and previous BAM studies showed that DFEE and DEE as well as TFEB and EB monolayers are polycrystalline and that their microcrystals keep autonomy up to high surface pressures. Compression of DFEE and TFEB monolayers sinters the microcrystals consisting of upright molecules, and this process seems to occur without significant change of the thinner hydration shells. The DEE and EB domains formed after spreading consist of closely packed molecules, whose chains are tilted toward next-nearest neighbors. Increasing surface pressure causes erection of the chains and a L2′-S or L2′-CS phase transition in both monolayers. Since the macroscopic orientation of the tilted chains in the microcrystals is random, the external force in the compression direction cannot directly erect all chains. However, compression of the microcrystals can increasingly dehydrate their heads thus decreasing the tilt angle of the chains. This process occurs continuously, which is typical for the tilting transition.

Acknowledgment. J.G.P. acknowledges the Alexander von Humboldt Foundation for the three-month stipend enabling this investigation. T.D.A. is indebted to the Max-Planck Society for the promotion stipend funding her participation in this work. We thank HASYLAB at DESY, Hamburg, for the beam time, and K. Kjaer and M. Weygand for the valuable help with setting up the experiment.

Supporting Information Available: In-plane Q_{xy} and out-of-plane Q_z components of the scattering vector for DFEE monolayers at different surface pressures and the full-width at half-maximum of the peaks (Table 1S), comparison of the calculated and experimental maxima of higher order diffraction peaks of the DFEE monolayer at 7 mN/m (Table 2S), and in-plane Q_{xy} and out-of-plane Q_z components of the scattering vector for DEE monolayers at different surface pressures and the full-width at half-maximum of the peaks (Table 3S). This material is available free of charge via the Internet at http://pubs.acs.org.

References and Notes

(1) *Fluorinated Surfactants*: *Synthesis*, *Properties*, *Applications*; Kiss, E., Ed.; Marcel Decker: New York, 1994.

(2) (a) Riess, J. G. *Colloids Surf., A* **1994**, *84*, 33−48. (b) Kraft, M. P.; Riess, J. G. *Biochimie* **1998**, *80*, 489−514.

(3) (a) Shinoda, K.; Nomura, T. *J. Phys. Chem*. **1980**, *84*, 36. (b) Funasaki, N.; Hada, S. *J. Phys. Chem.* **1983**, *87*, 342. (c) Kunitake, T.; Tawaki, S.; Nakashima, N. *Bull. Chem. Soc. Jpn*. **1983**, *56*, 3235. (d) Mukerjee, P. *Colloids Surf., A* **1994**, *84*, 1. (e) Elbert, R.; Lashewsky, A.; Ringsdorf, H. *J. Am. Chem. Soc*. **1985**, *107*, 4134. (f) Imae, T.; Takeshita, T.; Kati, M. *Langmuir* **2000**, *16*, 612.

(4) Ringsdorf, H.; Schlarb, B.; Venzmer, J. *Angew. Chem., Int. Ed. Engl.* **1988**, *27*, 113−158.

(5) (a) Fox, H. W. *J. Phys. Chem.* **1957**, *61*, 1058. (b) Barnett, M. K.; Zisman, W. A. *J. Phys. Chem.* **1963**, *67*, 1534. (c) Barnett, M. K.; Jarvis, N. L.; Zisman, W. A. *J. Phys. Chem.* **1964**, *68*, 3520. (d) Vogel, V.; Moebius, D. *J. Colloid Interface Sci.* **1988**, *12*6, 408. (e) Oliveira, O. N., Jr.; Taylor, D. M.; Lewis, T. J.; Salagno, S.; Stirling, Ch. J. M. *J. Chem. Soc., Faraday Trans. 1* **1989**, *85*, 1009.

(6) (a) Jacquemain, D.; Wolf, S. G.; Leveiller, F.; Lahav, M.; Leiserowitz, L.; Deutch, M.; Kjaer, K.; Als-Nielsen, J. *J. Am. Chem. Soc.* **1990**, *112*, 7724. (b) Barton S. W.; Bouloussa, O.; Rondelez, F.; Lin, B.; Novak, F.; Acero, A.; Rice, S. A. *J. Chem. Phys.* **1991**, *96*, 1343. (c) Acero, A. A.; Li, M.; Lin, B.; Rice, S. A.; Goldmann, M.; Azouz, I. B.; Goudot, A.; Rondelez, F. *J. Chem. Phys.* **1993**, *99*, 7214.

(7) Kaganer, V. M.; Moehwald. H.; Dutta, P. *Rev. Modern Phys.* **1999**, *71*, 779.

(8) (a) Petrov, J. G.; Möhwald, H. *J. Phys. Chem.* **1996**, *100*, 18458. (b) Petrov, J. G.; Polymeropoulos, E. E.; Möhwald, H. *Langmuir* **2000**, *16*, 7411. (c) Petrov, J. G.; Brezesinski, G.; Krasteva, N.; Möhwald, H. *Langmuir* **2002**, *17*, 4581.

(9) Brezesinski, G.; Dietrich, A.; Struth, B.; Boehm, C.; Bouwmann, W.; Kjaer, K.; Moehwald, H. *Chem. Phys. Lipids* **1995**, *76*, 145.

(10) (a) Paltauf, F.; Hauser, H.; Philips, M. C. *Biochim. Biophys. Acta* **1971**, *249*, 539. (b) Demchak, R. J.; Fort, T., Jr. *J. Colloid Interface Sci.* **1974,** *46*, 191. (c) Taylor, D. M.; Oliveira, O. N., Jr.; Morgan, H. *J. Colloid Interface Sci.* **1990**, *139*, 508.

(11) Petrov, J. G.; Andreeva, T. D.; Kurth, G.; Moehwald, H. In preparation.

(12) McConnell, H. M. *Annu. Rev. Phys. Chem.* **1991**, *42*, 171.

(13) Bondi, A. *J. Phys. Chem.* **1964**, *68*, 441.

(14) Mathieson, McL. A.; Welsh, H. K. *Acta Crystallogr.* **1965**, *18*, 953.

(15) McIntosh, T. J. *Biophys. J.* **1980**, *29*, 237.

(16) Levine, Y. K. *Prog. Biophys. Mol. Biol.* **1972**, *24*, 3. Levine, Y. K. *Prog. Biophys. Mol. Biol.* **1973**, *3*, 279.

(17) Tardieu, A.; Luzatti, V.; Reman, F. C. *J. Mol. Biol.* **1973**, *75*, 711.

(18) Hui, S. W. *Chem. Phys. Lipids* **1976**, *16*, 9.

(19) Boehm, C.; Moehwald, H.; Leiserowitz, L.; Als-Nielsen, J.; Kjaer, K. *Biophys. J.* **1993**, *64*, 553.

(20) Tenchov, B.; Kojnova, R.; Rappold, M.; Rapp, G. *Biochim. Biophys. Acta* **1999**, *1417*, 183.

(21) (a) Nagle, J. F.; Wiener, M. C. *Biochim. Biophys. Acta* **1988**, *942*, 1. (b) McIntosh, T. J.; Magid, A. D. In *Phospholipis Handbook*; Cevc, G., Ed.; Marcel Dekker, Inc.: New York, 1993; Chapter 15, p 553.

(22) Brezesinski, G.; Thoma, M.; Struth, B.; Möhwald, H. *J. Phys. Chem.* **1996**, *100*, 3126.

(23) Dahmen-Levinson, U.; Brezesinski, G.; Möhwald, H. *Thin Solid Films* **1998**, *327−329*, 616.

(24) Weidemann, G.; Vollhardt, D. *Biophys. J.* **1996**, *70*, 2758.

(25) Weidemann, G.; Brezesinski, G. M.; Vollhardt, D., Bringezu, F.; de Meijere, K.; Moehwald, H. *J. Phys. Chem.* **1998**, *102*, 148.